RSC Sustainability

Accepted Manuscript

This article can be cited before page numbers have been issued, to do this please use: D. Teja Nayak, V. K. Raja, A. Gangasalam, T. D. Khoa and W. Taweepreda, *RSC Sustain.*, 2025, DOI: 10.1039/D4SU00688G.

View Article Online
DOI: 10.1039/D4SU00688G

Sustainability spotlight

The amino acid (AA) and ionic liquids (ILs) incorporated on the cellulose acetate (CA) membranes to treat heavy metal ions from industrial wastewater as an efficient and effective membrane filtration technique. The potential impact of the presented work is significant, and it directly or indirectly supports several Sustainable Development Goals (SDGs): SDG 2, SDG 6, SDG 5, SDG 7, SDG 8, SDG 11, and SDG 14, by enabling efficient water recycling, accessing clean water, providing affordable and clean energy, fostering economic growth, enhancing resource efficiency, reducing waterborne diseases, reducing their burden of water collection, enhancing water management practices, enhancing water treatment.

View Article Online
DOI: 10.1039/D4SU00688G

A High-Performance Nanofiltration Membrane by Embedding Amino Acid and Ionic Liquids in the Cellulose Acetate for Heavy Metals Separation

D. Teja Nayak[1], Vinoth Kumar Raja[2], G. Arthanareeswaran[1*], Tran Dang Khoa[4], Wirach Taweepreda[5]

[1]*Membrane Research Laboratory, Department of Chemical Engineering, National Institute of Technology, Tiruchirappalli 620015, Tamil Nadu, India*

[2]*Membrane Research Laboratory, Department of Chemical Engineering, National Institute of Technology Andhra Pradesh, Tadepalligudem 534101, Andhra Pradesh, India*

[3]*Department of Nanobiotechnology, Faculty of Agricultural Technology, VNU-University of Engineering and Technology, Hanoi 122000, Vietnam*

[4]*Polymer Science Program, Division of Physical Science, Faculty of Science, Prince of Songkla University, Hat-Yai, Songkhla 90110, Thailand*

[*] Corresponding author.

E-mail address: arthanaree10@yahoo.com (G. Arthanareeswaran).

Tel: +91431-2503118; Fax: +91431-2500133.

View Article Online
DOI: 10.1039/D4SU00688G

Abstract

Water reclamation is necessary to meet the potable water demand. Heavy metals like iron, zinc, lead, and copper, particularly in water, pose significant toxicity risks to humans and other biological life. Over the last few years, the contamination level of these heavy metals in water and soils has increased alarmingly. On the other hand, membrane systems have emerged as a prominent approach to water reclamation. Subsequently, amino acid (AA) and ionic liquids (ILs) incorporated cellulose acetate (CA) membranes, which were fabricated using the phase inversion technique and effectively utilized for these metal separations. The membranes characterization by FTIR, SEM, TGA, and DSC exhibited the presence of various functional groups, change in surface morphologies, and improvement in thermal stabilities due to AA-IL, respectively. The pure water flux (PWF) was increased to 98 L/m^2 h at 4 bar pressure due to enhancement of hydrophilicity. Rejection percentage of heavy metal ions for AA–IL (0.5%) incorporated CA membranes was 94%. The rejection rates for 4 different heavy metal ions present in the industrial effluent were studied, and it was found that the rejection rate was 89,91,84, and 90% for copper, zinc, iron, and lead, respectively. AA–IL (0.5) incorporated the CA membrane's rejection capacity, which was observed to be the highest for all metals. The AA–IL incorporated CA membranes are efficient and effective for nanofiltration to treat heavy metal ions solution.

Keywords: industrial wastewater; amino acid; membrane separation; ionic liquids; cellulose acetate; nanofiltration

View Article Online
DOI: 10.1039/D4SU00688G

1. Introduction

Water is one of humankind's essential natural resources for various domestic and industrial applications. Large quantities of water are used in industries to produce or manufacture different products. Water utilization is increasing daily, which drives people to keep running behind the reusing of wastewater containing physical substances and organic contaminants. These modern-day wastewaters contain overwhelming metals. Heavy metals like copper, lead, zinc, magnesium, etc. surround us, and admission of these metals in small amounts has long-term impacts.(1) These metals in water have high concentrations and toxic properties that cause health issues.(2–6) The most ordinarily discovered substantial metals present in wastewater are arsenic, cadmium, chromium, copper, zinc, iron, and lead, which harm human well-being and the environment.(7) Various methodologies have been contemplated to advance filtration methods at the cheapest level to separate the metals. Increase in compelling advancement to diminish the amount of wastewater delivered and enhance the treated wastewater's nature.

During recent decades, membrane separation has been a proven technique that has dramatically improved with significant performance, and membrane commercial markets have been spreading rapidly worldwide. Membrane separation has been progressively utilized to treat inorganic waste because of its high effectiveness and low cost. There are diverse sorts of membrane filtration, such as ultrafiltration (UF), nanofiltration (NF), microfiltration (MF), and Reverse Osmosis (RO).(8) Using membranes in the profluent treatment process stacked with heavy metals has risen. The film forms (UF, MF, NF, and RO) were then utilized with different adequacy and selectivity.(9). In particular, cellulose acetate (CA), a biopolymer membrane, is one of the most commonly used membranes due to its high hydrophilicity, superior mechanical strength, and excellent film-forming capability during fabrication.(10)

Applying ionic liquids (ILs) has tremendous prominence because of their unique properties, such as less volatility, tuneable consistency, organic solvents, and their great extractability for

View Article Online
DOI: 10.1039/D4SU00688G

different natural mixes and metal particles, chiefly relying upon their uncommon structures. Ionic liquids are principally utilized for gas separations, and from the previous decade, ILs have likewise been used for heavy metal treatment.(11) The ILs exhibit a dual nature in salt form; it explored that the expulsion rate and limit of quaternary ammonium and phosphonium-based ILs connected to wastewater have initiated slime. In a study, the creation of the ILs utilized as the sorbing (extraction) specialist to impact the rejection rate of the substantial metals firmly. The examined ILs were astounding sorbing specialists for Zn, Ni, Cu, Cr, Cd, and Pb from actuated wastewater.(12) The metal ions transfer mechanism in ILs and the ionic nature of these ILs can result in different extraction mechanisms, including ion exchange, solvent ion-pair extraction, and a combination of both.(13) William et al. have reported that room-temperature ionic liquids consist of 1-ethyl-3-methylimidazolium (EMIM) cation and bis [(trifluoromethyl)sulfonyl] imide and anion stabilizes monomeric ligand-deficient transition-metal complexes (ruthenium, iron and titanium) via 4 different modes of binding: monodentate O or N coordination and bidentate N–O or O–O interaction.(13)

In this work, amino acids (AA) and ILs incorporated CA membranes are fabricated using the phase inversion technique for metal separation. The principle point of the present work is to expel the metal ions and deduce the concentration of iron (Fe), copper (Cu), Lead (Pb), and Zinc (Zn) from industrial wastewater through the synthesized AA–IL composite membranes using nanofiltration.

2. Materials and Methods

2.1. Materials

The CA polymer and N, N-dimethylformamide (DMF) were procured from Merck (India) Ltd., and 1 ethyl 3 methylimidazolium chloride was purchased from Tokyo Chemicals, Japan. Amino Acids (AAs), copper sulphate pentahydrate, and magnesium sulphate heptahydrate

were purchased from SRL Pvt. Ltd, India. All analytical grade chemicals have been used. Ultrapure water is produced using the Millipore pilot plant.

2.2. Fabrication of amino acids, ionic liquids incorporated CA membranes

The neat CA, amino acid, and ionic liquids incorporated composite CA membranes were synthesized using phase inversion-induced immersion precipitation.(14) A schematic representation of the fabrication of the CA/AA/IL membrane is shown in Figure 1. The composition of the casting solutions for all the fabricated membranes is given in Table 1. AA, ILs, and AA–IL loading percentages were kept at 0.5%, 1%, and 5% of CA, respectively. AA, IL, and AA–IL were added to DMF, and through sonication, it was dispersed well for 1 h using an ultrasonicator to enhance the solution homogeneity. After homogenisation, CA powder was dissolved in the DMF solution for 4 h by mechanical stirring. Then, the dope solution was placed in ultrasonication for 30 min to form a complete dispersion of AA and IL. The air bubbles were removed from the casting solution and were cast onto a glass plate, which was finely leveled with a casting knife of 400 μm thickness. Eventually, the thin film is dipped in distilled water and kept at 10°C to ensure the complete phase inversion.(15) The membranes are named by neat CA membrane as M1, CA-(1%) of AA as M2, CA-(5%) of IL, (1%) of AA as M3, CA-(0.5%) of AA as M4.

2.3. Characterisation of membranes

2.3.1. Fourier Transform Infrared (FTIR) spectroscopy

The change in chemical structure and AA-ILs functional group was analysed using ATR interfaced Fourier transform infrared (FTIR) spectrophotometer (Thermo Scientific Nicolet iS5 FT-IR spectrometer). The change in chemical structure can be observed by means of wavenumber drift against the percentage transmittance, and the samples were collected over the spectral region of wavelengths from 400 to 4000 cm^{-1}. (16)

2.3.2. Thermogravimetric analysis

View Article Online
DOI: 10.1039/D4SU00688G

The thermal stability of the prepared neat CA and AA, IL incorporated CA membranes were examined using a thermogravimetric analyser (DGT 2000, Perkin Elmer, 2915 133rd Street West, USA). All the fabricated membrane samples were allowed to dry in a vacuum oven at 60 °C for 24 h before testing. The prepared membrane samples were analysed with a heating rate of 10 °C/min from 50 to 700 °C under a nitrogen atmosphere.[11]

Differential scanning calorimetry

DSC is used to quantify changes in heat flows related to material changes. DSC estimation provides both quantitative and subjective information on endothermic and exothermic forms. DSC is ordinarily used to decide the glass transition temperature and melting point of crystalline for polymeric materials. All the fabricated membrane samples were dried in a vacuum oven at 60 °C. The samples were analysed from 50 - 700 °C at a heating rate of 10 °C/min under nitrogen air.(17)

2.3.3. Surface morphology

The neat CA and composite CA, AA, and IL membrane cross-sections were scanned with a scanning electron microscope (SEM) with energy-dispersive X-ray (VEGA 3, TESCAN, USA). The cross-sectional image of neat CA, AA, and IL membranes was taken by keeping the samples in the cathode field emission at 1–15 kV. Before taking the cross-sectional images, all the fabricated membrane samples were frozen in liquid nitrogen and fractured. The manufactured membrane samples were cut into required pieces, cleaned with filter paper, and kept in an air drier. The dried pieces of membrane samples were varnished with gold by blabbering to make them conductive.

2.3.4. Surface topology of fabricated membranes

Atomic force microscopy (AFM) is used to identify the surface roughness parameter by tapping mode method (Nano surf scanning probe optical microscope, easy scan Ⅱ, USA).(18)

2.3.5. Membrane porosity and pore size

View Article Online
DOI: 10.1039/D4SU00688G

All the fabricated samples were slashed into specific sizes and then mopped with filter paper. After taking wet weight, the samples were allowed to dry in a vacuum oven at 60°C for one day. The porosity (ε) is determined from the dry and wet weights of the membranes using the following equation [Eq. 1].(19)

$$\varepsilon = \left(\frac{\frac{\omega_1 - \omega_2}{d_w}}{\frac{(\omega_1 - \omega_2)}{d_w} + \left(\frac{\omega_2}{d_p}\right)} \right) \qquad \text{[Eq.1]}$$

where, ω_1 − the wet weight of the fabricated membrane sample (g), ω_2 – the dry weight of the fabricated membrane sample (g), d_w – water density (kg/cm^3), d_p – density polymer (kg/cm^3) By using the filtration velocity technique, the mean radius of the fabricated membrane pore was calculated using the Guiraud-Elford-Ferry (GEF) equation [Eq. 2]. (20)

$$r_m = \sqrt{\left(\frac{(2.9 - 1.75\varepsilon)\ 8Ql\eta}{\varepsilon\ A\ \Delta P}\right)} \qquad \text{[Eq. 2]}$$

where, Q − the flow rate of the permeate (m^3/s), A − the effective cross-sectional area of the membrane (m^2), ΔP − the transmembrane pressure (Pa), η − the dynamic viscosity of the water (Pa s), l − the thickness of the membrane (m).

2.3.7. Contact angle measurement

The hydrophilicity of neat CA, AA, and IL-incorporated composite CA membranes was examined using contact angle measurement. The goniometer (demonstrate rame-hart 250-F1, USA) was used for contact angle assurance using the sessile drop technique for the fabricated membranes. About 5 µL distilled water drop is infused on the top surface of a dry membrane at five unique areas using a micro syringe. The contact angle value was estimated from the independent distilled water droplets in the five different regions, which decide the hydrophilicity of the layer.

View Article Online
DOI: 10.1039/D4SU00688G

2.4. Work of adhesion

The work of adhesion (ΔG_S) is called surface free energy. This assesses the firmness of contact between membrane and surface water. W_a is the amount of work needed to segregate two different liquid-solid or liquid-liquid phase boundary phases from each other. (14)

W_a is calculated from the Youngs equation using the contact angle [Eq. 3].

$$-\Delta GS = (1 + cos \propto)\, \gamma \qquad \text{[Eq. 3]}$$

where, $\propto$ is the contact angle of the sample and γ represents the water surface tension (72.8 mJ/m^2).

2.5. Hydration capacity

Hydration capacity was calculated by the difference in wet weight (a membrane immersed in distilled water at 30 °C for 1 day) and dry weight of the fabricated membrane of its thickness and total surface area of the membrane [Eq.4].

$$\text{Hydration capacity} = \frac{Ww - Wd}{A \times l}\ (\text{m J/m}^2) \qquad \text{[Eq. 4]}$$

2.6. Permeation studies

The nanofiltration experiment was conducted for pure water flux and heavy metal solution with the pressure of 4 bar, nitrogen gas as pressure developing medium using neat CA membrane (M1) and AA, IL incorporated CA membranes (M2, M3, and M4). The permeation of neat CA and AA, ILs incorporated composite membranes were studied for pure water and heavy metal solution at 4 bar pressure with a pH 7 using a dead-end nanofiltration cell (model HP4750 STIRRED CELL, AVENUE S KENT, USA), shown in Figure 2 with an effective membrane area of 14.6 cm^2. Initially, membrane compaction was done to collect the steady-state permeates. Once a steady state was observed, the permeate was collected for a period of time for each membrane. The flux (J_w) of the membrane was calculated using the equation [Eq.5].

$$j_w = \frac{V}{A \times \Delta t} \qquad \text{[Eq.5]}$$

View Article Online
DOI: 10.1039/D4SU00688G

where, J_w = pure water flux (L/m^{2}hr), V = permeating volume (L), A = effective membrane area (m^2), and Δt = permeation time (h).

2.6.1. Permeation and rejection performance at different operating conditions

The changes in permeate fluxes and pure water flux were studied by varying the pressure. Also, the rejection rates of magnesium and copper for these fabricated membranes were scrutinized with synthetic wastewater using nanofiltration. The experiment was conducted under three different operating pressures: 2, 4, and 6 MPa, with a pH of 4 and 7 as these factors are critical in influencing permeate flux, rejection efficiency, solution chemistry, and the membrane's surface charge.(21) All the experiments were conducted in triplicate.

2.7. Treatment of wastewater from metal ion-based industry

The wastewater utilized in the process was procured from the metal industry, Tiruchirappalli, Tamil Nadu, India. The composition and characteristics of wastewater is presented in Table 2. The concentration of heavy metals was tested using atomic absorption spectroscopy (Systronics Limited, India). Table 2 shows that industrial wastewater generally has higher concentrations of iron, copper, lead, and zinc particles than different cations.[6] The rejection percentage of industrial wastewater for both neat CA and CA, AA, IL membranes was evaluated by the following equation [Eq.6].

$$R = \left(1 - \frac{C_f}{C_p}\right) \times 100 \qquad \text{[Eq.6]}$$

Where, C_f -feed concentrations of the heavy metal solutions, C_p -permeate concentrations of the heavy metal solutions.

3. Results and Discussions

3.1.Confirmation of AA, IL in polymer membrane

The FTIR spectra of the neat CA (M1), amino acid, and ionic liquid grafted membranes with different compositions (M2, M3, and M4) are shown in Figure 3. The major absorbance bands

View Article Online
DOI: 10.1039/D4SU00688G

are delivered at 3400 cm^{-1}, corresponding to the OH group's stretching vibration. Compared to the neat membrane, new characteristic peaks of the CA–AA membranes at 3388 cm^{-1} was the stretching vibration of N–H, which indicates the amino acid salt has been successfully instigated into the neat CA membrane. The band at 450 cm^{-1} is because of the alkyl halide of IL, confirming the presence of IL. Similarly, no specific changes were observed in the spectra when AA–IL is grafted onto the surface of neat CA, i.e., due to the neat CA having functional groups similar to the CA–IL–AA membrane. The peaks observed at 2892 cm^{-1} have been reported to be antisymmetric CH_3 stretching due to the presence of the imidazolium part of ILs. (22)

3.2. Surface morphology of the fabricated membrane

Figures 4 and 5 identify the morphological structure that appeared in all fabricated membranes. The neat CA membrane's surface morphology is smooth and observed to have a non-porous structure. CA–AA surface is totally rough when compared to that of the neat membrane due to the presence of amino acids where complete dispersion was observed, and the presence of voids can be seen. (CA–AA–IL–5%) membrane and (CA–AA–IL–0.5%) surfaces have flattened shapes and seem to have rough surfaces along with micropores.

Figure 5 shows the cross-section morphology with an asymmetric structure. The neat CA membrane shows the presence of macro voids with a thick skin layer on the top. The presence of large finger-like structures with a decrease in the thickness of the skin layer is due to the addition of AA. Adding ionic liquid and amino acid to the CA membrane with two different compositions shows the increase of macro voids due to the increased addition of ionic liquid percentage, which decreases the surface skin layer from a dense layer to a thin layer (Figure 5). The primary role of IL additives is to increase the membrane's hydrophilicity.(22)

3.3. Surface Topology of fabricated membrane

Figure 6 shows the AFM images of CA, CA/AA, and CA/IL membranes given by tapping mode. The neat membrane was observed to be rough on the surface, with many small craters

View Article Online
DOI: 10.1039/D4SU00688G

and valley structures**.** The neat CA membrane also showed high hydrophilicity, as evidenced by a contact angle of 51.18º, which contributes to its higher water flux.(23) The AA-embedded polymeric membrane was observed to have a smooth and flat surface with a decrease in crater valley surface compared to the neat CA membrane. The depletion in the roughness of the membranes was clearly due to the doping of AA into the neat CA.(22) This smoothing effect resulted in a higher hydrophobicity of membrane M2, as indicated by a contact angle of 68.39 º. On the other hand, the incorporation of IL into membrane M3 resulted in a rougher surface, which enhanced hydrophilicity, as supported by a contact angle of 51.94º (24).

3.4. Contact angle measurement

Table 3 shows the contact angles of the fabricated membrane (Figure 7). The neat CA membrane has a contact angle of 51.18°. When compared to the neat CA membrane, the contact angle of the amino acid incorporated membrane has been increased to 68.39°. This is due to the Rose Petal Effect **(**The microstructure controls the contact angle hysteresis, whereas the nanostructure provides high CA. As a result, a rose petal can exhibit typical lotus effect properties (high CA and low CA hysteresis) or petal effect properties (high CA and high CA hysteresis. Artificial surfaces that mimic rose petals were investigated, and similar behavior was found,(25) which explains the hydrophobicity of amino acids in the case of CA–AA–ILs membranes contact angles have been increased to 63.06°, and this might be due to the presence of the amino acid group, i.e., contact angle tends to increase as the pH varies from alkaline to acid. The composite membrane has become hydrophilic because of the increase in the loading of 5% chlorine-based ionic liquid. This could be credited to the hydrophilic nature of chlorine-based ionic liquid. (26) At higher concentration of ionic liquid the decrease in contact angle enhances membrane hydrophilicity, leading to the formation of a stable hydration layer over the surface. This hydration layer acts as a protective barrier, repelling foulants such as proteins, bacteria, and organic matter by preventing their direct

View Article Online
DOI: 10.1039/D4SU00688G

adhesion. The presence of a well-structured hydration layer reduces surface energy and minimizes hydrophobic interactions, thereby improving antifouling efficiency (27). The increase in contact angle due to the incorporation of amino acid demonstrates the hydrophobicity of membrane. Halan et al reported the similar effect of charge and hydrophilicity on the antifouling properties of polyester membrane (28). Thus, the synergistic effect of amino acids and ionic liquids not only modifies the membrane's surface wettability but also improves its antifouling properties, making it more resistant to both organic and inorganic foulants.

3.5.Thermo gravimetric analysis

The thermal properties of the membranes were determined using thermogravimetric analysis (TGA), as shown in Figure 8. All the fabricated membranes have better thermal stability up to 330°C. The weight loss is 4% up to 330 °C for neat membrane (M1). Adding ionic liquid and amino acid influences the membranes' thermal stability. The other membrane M2 has a slightly lower weight loss percentage (3%) than the neat membrane (M1), indicating improved thermal stability.

The membranes M3 (CA–AA–IL–5%) and M4 (CA–AA–IL–0.5%) have less thermal stability because of chloride ions present within the membrane matrix and tend to degrade with weight loss of 6% up to 145°C. Later, CA–AA is stable up to 330°C due to the presence of amino acid, and the degradation from 330°C is due to the CA membrane.(23) The observed thermal stability enhancements suggest that the interactions between amino acids and the CA matrix improve polymer chain rigidity, thereby delaying thermal degradation (29). Additionally, the ionic liquid incorporation influences membrane decomposition behavior, which aligns with the findings of Lea Chancelier. The impact of the alkyl chain length and the presence of functional groups and unsaturation was evaluated, revealing that the thermal behavior is governed by Van der Waals interactions between alkyl chains and inter- and intra-molecular coulombic interactions such as hydrogen bonding. (30)

View Article Online
DOI: 10.1039/D4SU00688G

3.6. Differential scanning calorimetry

DSC is a technique where thermal analysis is carried out to measure heat flow changes related to material transitions. From Figure 9, all the membranes show exothermic peaks on the thermogram associated with melting the membrane samples. The T_g value of neat CA was observed to be 64°C, whereas the amino acid incorporated membrane CA–AA has 91°C, indicating enhanced thermal stability. This increase in Tg is attributed to strong interactions between amino acid molecules and the CA polymer matrix. Additionally, the DSC results further validate the TGA findings, as the improved thermal stability of modified membranes correlates with increased Tg values.

It could be expected that a decrease in the concentration of ionic liquid, explained by Lea Chancelier,[20] will lead to a reduction in the melting point of the membrane. (CA–AA–IL–5%) has a higher melting point compared to that of (CA–AA–IL–0.5%), which suggests that a higher ionic liquid concentration influences intermolecular interactions and phase transitions. This correlation between thermal stability, decomposition behavior, and glass transition temperature further supports the structural modifications induced by amino acid and ionic liquid incorporation, demonstrating their influence on the membrane's thermal properties.

3.7. Pore size and porosity of membranes

The porosity of the (CA–AA–IL–5%) incorporated CA membrane is increasing from 36.42 to 44.15 % with the increasing concentration of ILs in the CA membranes from 0 to 5%. Increasing porosity of the membranes impacts the membrane flux.(31) The pore size of the membranes is gradually rising from 3.16 to 3.91nm with the increasing concentration of AA, IL from 0 to 5% in the CA membrane, shown in Table 4. The membrane pores have a positive charge due to the incorporation of ionic liquid, which reduces wastewater's viscosity, allowing it to pass freely. Consequently, the permeate flux increases. The formation of pores in the membrane surface enhances the permeability of membranes.(18) For (CA–AA–IL–0.5%) incorporated CA membrane, the translocation of hydrophobic amino acids may involve a

View Article Online
DOI: 10.1039/D5SU00688G

modest amount of partitioning into the membrane interior, as well as translocation through transient defects; as a result, small pores were formed which increases the rejection rate.

3.8. Permeability of membranes

The pure water flux of neat CA and AA–IL membranes is listed in Table 5 (Figure 10). When applying 4 bar pressure to membranes, the flux increased from 75 L/m^2 h to 98 L/m^2 h, and the rising concentration of AA influenced the increasing permeability of CA membranes–IL in CA membranes. It confirms that adding AA–IL effectively enhanced CA membranes' hydrophilicity and pore formation. It is because during AA-IL membrane modification, the ILs replace part of the polymer, regulating the chemical and hydrogen bonding of the CA chains and enhance hydrophilicity and pore formation. Although the mean pore sizes of CA+AA (1%) +IL (5%) membrane only increase marginally compared to the Neat CA membrane. It means the flux improvement happened due to the enhanced hydrophilicity and the possibly larger pore size on the surfaces of the AA-IL membranes which allow to transport of water through surface/internal pores of AA-IL membranes more quickly.

The incorporation of amino acids and ionic liquids into cellulose acetate membranes enhances hydrophilicity, leading to improved water flux and antifouling properties. (32) However, increased hydrophilicity can sometimes compromise mechanical strength due to higher water absorption, which may weaken the polymer matrix. Conversely, amino acid incorporation can enhance mechanical stability through hydrogen bonding and intermolecular interactions, partially mitigating this effect. Thus, optimizing the concentration of these additives is crucial to achieving a balance between high water permeability and sufficient mechanical robustness for long-term application.

3.9. Nanofiltration performance at different pressures and pH

View Article Online
DOI: 10.1039/D4SU00688G

The NF performance for copper and magnesium metal ion solutions at different pressures and pH are conducted, and the results are presented in Figure 11. The operating pressure increases from 2 to 6 bar and pH from 4,7. It was observed that both synthetic and real wastewater's flux values increased, and the rejection rates decreased. At all operating pressures, copper and magnesium solutions had the highest flux at a pH of 4. The highest flux was 209 L/m^{2}h for the (CA–AA–IL–5%) membrane, while 127 L/m^{2}h was observed for the neat CA membrane for copper metal ion solution. It was observed to be 152 L/m^{2}h for (CA–AA–IL–5%) membrane while 111 L/m^{2}h for Neat CA membrane for magnesium metal ion solution. A similar type of flux values were found for 4 bar pressure. The highest flux was observed for copper metal ions at 6 bar pressure at pH 4 compared to pH 7. It was observed to be 320 L/m^{2}h (CA–AA–IL–5%) membrane while 279 L/m^{2}h was observed for neat CA membrane for copper metal ion solution. It was observed to be 295 L/m^{2}h for (CA–AA–IL–5%) membrane while 189 L/m^{2}h for Neat CA membrane for Magnesium metal ion solution. It can be seen that all of the pure water flux (PWF) and NF performances have the same variation trend. Figure 12 gives the flux values of the industrial wastewater. Compared with the neat membrane, the Ionic liquid (5%) and amino acid (1%) incorporated membrane have higher flux values than the neat membrane due to the hydrophilic nature of the IL-embedded membrane. The flux of (CA–AA–IL–5%) was observed to be very high, 78 (L/ m^2 h), because of the presence of chloride-based ionic liquid. The (CA–AA–IL–0.5%) membrane was observed to have a very low flux of 33 (L/m^2 h) compared to that of (CA–AA–IL–0.5%) because of lower values of IL compared to other membranes. It can certainly be observed that the pure water and permeate flux for industrial wastewater treatment increases directly when operating pressure increases.

Consequently, the flux values are decreasing as the pH increases. A similar change was observed elsewhere (1,31). Figure 11 shows that increased operating pressure results in overcoming the resistance of the membrane and enhancing the driving force. Besides, the

View Article Online
DOI: 10.1039/D4SU00688G

difference between the permeate and pure water flux for industrial wastewater treatment increased with the operating pressure because concentration polarization is negligible under lower operating pressures but not at higher pressures. When the operating pressure increases, concentration polarization also tends to increase, increasing the osmotic pressure that leads to a decline in the total effective pressure, decreasing permeate flux, and increasing rejection rates.(33) When low pressures are present, surface forces play more prominent role than the training forces. Moreover, the solvent flux increases as pressure increases and tends to decrease in the permeate solute concentration by increasing its rejection rate. After certain pressure levels, the surface forces of the solute become weak compared to the training forces; thus, the transportation increases in the solute and reduces rejection rates.(34)

3.10. Effluent rejection

The rejection performance of these fabricated membranes was studied using synthetic metal ion solution for Cu and Mg (1000 ppm) varying pressure and pH for industrial wastewater. The studies were conducted at a pressure of 4 bar and pH 7 for industrial wastewater, whereas pressure and pH varied for synthetic metal ion solution. It is shown in Table 5 and Figure 13. Rejection experiments were carried out at pH 7. Higher Cu, Zn rejection % was observed for (CA–AA–IL–5%) membrane of 90 %, 91 % when compared to all other membranes; this might be due to the low porosity size, surface blocks, and rejects of the metal ions passing through the surface. A higher rejection was observed at pH 7 for the AA-embedded polymeric membrane, i.e., 82 %, which is explained by the membrane's pore-size modification mechanisms and SEM images. Additionally, the Donnan exclusion effect plays a critical role, where the fixed charged groups on the membrane surface induce electrostatic repulsion with co-ions(35). This electrostatic repulsion effect is particularly pronounced for multivalent metal ions, contributing to the observed higher rejection rates for copper and zinc compared to magnesium or iron. The highest rejection was observed for copper at 4 bar pressure at pH 7 compared to that of pH 4. It was observed to be 88 % for (CA–AA–IL–0.5%) embedded

View Article Online
DOI: 10.1039/D4SU00688G

polymeric membrane, while 58% was observed for neat CA membrane for Copper solution at a pH of 7. It was observed to be 83% for (CA–AA–IL–0.5%) embedded polymeric membrane while 54% for Neat CA membrane for Magnesium metal ion solution. The highest rejection was observed for copper at 6 bar pressure at pH 7 compared to that of pH 4. It was observed to be 93% for (CA–AA–IL–0.5%) embedded polymeric membrane, while 62% was observed for the Neat CA membrane for Copper solution at a pH of 7. It was observed to be 89% for (CA–AA–IL–5%) embedded polymeric membrane while 44% for Neat CA membrane for magnesium metal ion solution, at pH of 7. Consequently, as pH changes from pH 4 to 7, the membrane pore size has a reducing positive charge, and as a result, there is a decline in the permeate flux, which leads to a gradual increase in the rejection rate of metal ion solution. It is observed that the rejection performance slowly increases with a rise in pH; higher rejection values were seen for pH 7 on average.

The operating pressure influence on the magnesium and Copper rejection rates using the fabricated membranes from industrial wastewater is shown in Figure 14. As the operating pressure increases, there is an increase in the rejection rates of all heavy metals, which can be explained as follows: The low rejection rate was observed due to low operating pressure; it can be observed higher diffusive transport than convective transport through the membranes. Convective transport becomes more prominent compared to diffusive transport, which reduces the solute concentration in the permeate, resulting in a hike in the rejection rate of the solute; (36) however, as the operating pressure increases, concentration polarization will also tends to increase, which leads to a decline in solute dismissal rates by a reduction in the charge impact. The subsequent improved heavy metal rejection rates with increasing operating pressure demonstrate that the increase in convective transport dominates the solute rejection behavior at all operating pressures. According to the Donnan exclusion principle, more rejection rates are observed for heavy metal with high valance charge due to the stronger

View Article Online
DOI: 10.1039/D4SU00688G

electrostatic repulsion exerted by the membrane.(37) Therefore, copper and zinc rejection rates are higher than that of remaining metal ions.

Rejection studies were carried out for industrial wastewater using nanofiltration set up with all four different fabricated membranes at a pressure of 4 bar and pH. The rejection rates for 4 different metals are shown in Table 6. The highest rejection rate for iron was 89% for the (CA–AA–IL–0.5%) membrane compared to other membranes. The highest rejection rate for Zinc was 91% for both CA-AA and (CA–AA–IL–0.5%) membranes compared to two other membranes. The highest rejection rate for Lead was found to be 84% for the (CA–AA–IL–0.5%) membrane compared to other membranes. The highest rejection rate for copper was found to be 90 % for the (CA–AA–IL–0.5%) membrane compared to other membranes. Notably, there is a 90% rejection when the adhesion strength between copper and the polymer to create a strong and reliable connection.(38) The obtained rejection rates of heavy metal ions were comparable to those reported in other research studies. For instance, a metal-organic framework-embedded CA membrane achieved rejection rates of 77% for Co(II) and 53% for Cu (II).(39) Similarly, CA membranes produced from cigarette butt recycling demonstrated rejection efficiencies of 85.2%, 88.4%, and 85.3% for lead, chromium, and cadmium, respectively.(40). Additionally, another study reported the removal efficiencies of Fe^{2+}, Ba^{2+}, and Al^{3+} from dam water using CA membranes as 91.95%, 83.33%, and 59.37%, respectively. (41). These comparisons highlight the competitive performance of the fabricated membranes in heavy metal removal.

One of the pictorial representations of feed and permeate samples of the industrial wastewater treatment carried out in this study is presented in Figure 15. In this study, the incorporation of ILs enhanced the hydrophilicity of the membranes, improving water flux and antifouling properties. However, excessive hydrophilicity may sometimes impact the mechanical strength and durability of the membranes. By optimizing the concentration of AA and IL, a balance was achieved, ensuring improved permeability while maintaining sufficient structural

View Article Online
DOI: 10.1039/D4SU00688G

integrity for effective nanofiltration applications. AA-LLs have also been considered to be environment friendly and greener than conventional solvent and have negligible leach out during membrane formation. In addition, synergistic effect of both AA and ILs can be influenced to selectively remove metal substances, making them useful for the removal of metal ions from effluent. Overall, the combination of AA and LLs have great potential for use in sustainable and efficient metal ions separation processes.

4. Conclusion

The AA-IL incorporated CA membranes were prepared using the phase inversion method in this work. The membranes were characterized by various methods such as SEM, contact angle, DSC, and TGA. The contact angle disclosed that the membranes' wettability significantly varied by adding AA and ILs. The surface morphology of fabricated membranes also varied compared to neat CA membrane. TGA and DSC exhibited that the thermal stability of the fabricated membranes was altered due to the addition of AA–IL. The AA–IL enhanced the hydrophilicity, which is confirmed by the contact angles of the membranes and also by pure water flux values. Further, nanofiltration (NF) experiments were conducted to separate heavy metals such as copper, zinc, iron, and lead from industrial wastewater at different pH levels and pressures on permeate flux, and rejection rates were studied for industrial wastewater. The developed membrane potentially rejected copper, zinc, iron, and lead 89%, 91%, 84%, and 90%, respectively, for 0.5% of AA and IL incorporation. The rejection of heavy metal ions was significantly improved with the inclusion of AA and ILs. Notably, the fabricated membranes demonstrate promising performance for heavy metal removal while being environmentally friendly. The use of cellulose acetate, amino acids, and ionic liquids not only enhances membrane properties but also aligns with sustainability goals, considering their renewable nature, reducing reliance on hazardous chemicals, and minimal environmental impact during fabrication. Furthermore, the cost-effectiveness, availability of

View Article Online
DOI: 10.1039/D4SU00688G

materials and the simplicity of the fabrication process suggest that the membrane fabrication process can be scaled up for large-scale industrial applications.

References

1. Arthanareeswaran G, Thanikaivelan P, Jaya N, Mohan D, Raajenthiren M. Removal of chromium from aqueous solution using cellulose acetate and sulfonated poly(ether ether ketone) blend ultrafiltration membranes. J Hazard Mater. 2007;139(1):44–9.
2. Shrestha R, Ban S, Devkota S, Sharma S, Joshi R, Tiwari AP, et al. Technological trends in heavy metals removal from industrial wastewater: A review. J Environ Chem Eng. 2021;9(4).
3. Singhal A. Heavy metals in drinking water and their impact on human health. Asian J Res Soc Sci Humanit. 2021;11(11):586–91.
4. Li M, Shi Q, Song N, Xiao Y, Wang L, Chen Z, et al. Current trends in the detection and removal of heavy metal ions using functional materials. Chem Soc Rev. 2023;52(17):5827–60.
5. Tang Y, Zhang L, Ge X, Zhang Y, Liu Y, Wang J. A mild one-step method to fabricate graphene oxide cross-linked with dopamine/polyethyleneimine (GO@DA/PEI) composite membranes with an ultrahigh flux for heavy metal ion removal. Sep Purif Technol. 2024;339:126618.
6. Qasem NAA, Mohammed RH, Lawal DU. Removal of heavy metal ions from wastewater: a comprehensive and critical review. npj Clean Water. 2021;4(1).
7. Fu F, Wang Q. Removal of heavy metal ions from wastewaters: A review. J Environ Manage. 2011;92(3):407–18.
8. Rossignol N, Vandanjon L, Jaouen P, Quéméneur F. Membrane technology for the continuous separation microalgae/culture medium: compared performances of cross-flow microfiltration and ultrafiltration. Aquac Eng. 1999;20:191–208.

View Article Online
DOI: 10.1039/D4SU00688G

436 9. Salem H., Eweida E., Faraq A. Heavy Metals in Drinking Water and Their
437 Environmental Impact on Human Health. Cairo Univ. 2000;542–56.
438 10. Islam MD, Uddin FJ, Rashid TU, Shahruzzaman M. Cellulose acetate-based membrane
439 for wastewater treatment—A state-of-the-art review. Mater Adv. 2023;4(18):4054–
440 102.
441 11. Han D, Row KH. Recent applications of ionic liquids in separation technology.
442 Molecules. 2010;15(4):2405–26.
443 12. Fuerhacker M, Haile TM, Kogelnig D, Stojanovic A, Keppler B. Application of ionic
444 liquids for the removal of heavy metals from wastewater and activated sludge. Water
445 Sci Technol. 2012;65(10):1765–73.
446 13. Williams DB, Stoll ME, Scott BL, Costa A, Oldham WJ. Coordination chemistry of the
447 bis (trifluoromethylsulfonyl) imide anion : molecular interactions in room temperature
448 ionic liquids. 2005;613(1):1438–40.
449 14. Aditya Kiran S, Lukka Thuyavan Y, Arthanareeswaran G, Matsuura T, Ismail AF.
450 Impact of graphene oxide embedded polyethersulfone membranes for the effective
451 treatment of distillery effluent. Chem Eng J. 2016;286:528–37.
452 15. Arthanareeswaran G, Srinivasan K, Mahendran R, Mohan D, Rajendran M, Mohan V.
453 Studies on cellulose acetate and sulfonated poly(ether ether ketone) blend ultrafiltration
454 membranes. Eur Polym J. 2004;40(4):751–62.
455 16. Hafeez S, Fan X, Hussain A. A Kinetic Study of CO2 Adsorption in Cellulose Acetate
456 Membranes. Int J Environ Sci Dev. 2015;6(10):755–9.
457 17. Xing P, Robertson GP, Guiver MD, Mikhailenko SD, Wang K, Kaliaguine S. Synthesis
458 and characterization of sulfonated poly(ether ether ketone) for proton exchange
459 membranes. J Memb Sci. 2004;229(1–2):95–106.
460 18. R SK, Arthanareeswaran G, Y LT, Ismail AF. Journal of the Taiwan Institute of
461 Chemical Engineers Enhancement of permeability and antibiofouling properties of

polyethersulfone (PES) membrane through incorporation of quorum sensing inhibition (QSI) compound. J Taiwan Inst Chem Eng. 2017;72:200–12.

19. Gnanasekaran G, G A, Mok YS. A high-flux metal-organic framework membrane (PSF/MIL-100 (Fe)) for the removal of microplastics adsorbing dye contaminants from textile wastewater. Sep Purif Technol. 2021;277(September):119655.

20. Zhao F, Chu H, Yu Z, Jiang S, Zhao X, Zhou X, et al. The filtration and fouling performance of membranes with different pore sizes in algae harvesting. Sci Total Environ. 2017;587–588:87–93.

21. Shukla AK, Alam J, Ansari MA, Alhoshan M, Alam M, Kaushik A. Selective ion removal and antibacterial activity of silver-doped multi-walled carbon nanotube / polyphenylsulfone nanocomposite membranes. Mater Chem Phys. 2019;233(April):102–12.

22. Hu W, Ma Y, Zhan Z, Hussain D, Hu C. Robotic Intracellular Electrochemical Sensing for Adherent Cells. Cyborg Bionic Syst. 2022;2022.

23. Zhu WP, Gao J, Sun SP, Zhang S, Chung TS. Poly(amidoamine) dendrimer (PAMAM) grafted on thin film composite (TFC) nanofiltration (NF) hollow fiber membranes for heavy metal removal. J Memb Sci. 2015;487:117–26.

24. Alhoshan M, Alam J, Shukla AK, Hamid AA. Polyphenylsulfone membrane blended with polyaniline for nanofiltration promising for removing heavy metals (Cd2+/Pb2+) from wastewater. J Mater Res Technol. 2023;24:6034–47.

25. Wang Z, Fernández-Blanco C, Chen J, Veiga MC, Kennes C. Effect of electron acceptors on product selectivity and carbon flux in carbon chain elongation with Megasphaera hexanoica. Sci Total Environ. 2024;912(December 2023).

26. Tan K, Li C, Meng H, Wang Z. Improvement of hydrophobicity of ionic liquids by partial chlorination and fluorination of the cation. Chinese J Chem. 2009;27(1):174–8.

27. Xiong Z, Liu J, Yang Y, Lai Q, Wu X, Yang J, et al. Reinforcing hydration layer on

membrane surface via nano-capturing and hydrothermal crosslinking for fouling reduction. J Memb Sci [Internet]. 2022;644(September 2021):120076. Available from: https://doi.org/10.1016/j.memsci.2021.120076

28. Mohamed H, Hudziak S, Arumuganathan V, Meng Z, Coppens MO. Effects of charge and hydrophilicity on the anti-fouling properties of kidney-inspired, polyester membranes. Mol Syst Des Eng. 2020;5(7):1219–29.

29. Alotaibi KM, Shukla AK, Bajuayfir E, Alotaibi AA, Mrad MH, Gomaa FA, et al. Ultrasound-assisted synthesis of MSNs/PS nanocomposite membranes for effective removal of Cd2+ and Pb2+ ions from aqueous solutions. Ultrason Sonochem. 2023;98(June):106497.

30. Boyron O, Gutel T, Commission AE, Santini CC. Thermal stability of imidazolium-based ionic liquids Thermal stability of imidazolium-based ionic liquids. 2016;(August 2018).

31. Hwang T, Oh YK, Kim B, Han JI. Dramatic improvement of membrane performance for microalgae harvesting with a simple bubble-generator plate. Bioresour Technol. 2015;

32. Fallah Z, Zare EN, Khan MA, Iftekhar S, Ghomi M, Sharifi E, et al. Ionic liquid-based antimicrobial materials for water treatment, air filtration, food packaging and anticorrosion coatings. Adv Colloid Interface Sci. 2021;294.

33. Wang X, Zhou K, Ma Z, Lu X, Wang L, Wang Z, et al. Preparation and characterization of novel polyvinylidene fluoride/2-aminobenzothiazole modified ultrafiltration membrane for the removal of Cr(VI) in wastewater. Polymers (Basel). 2018;10(1).

34. Abidi A, Gherraf N, Ladjel S, Rabiller-Baudry M, Bouchami T. Effect of operating parameters on the selectivity of nanofiltration phosphates transfer through a Nanomax-50 membrane. Arab J Chem. 2016;9:S334–41.

514 35. Shukla AK, Alam J, Alhoshan M, Arockiasamy Dass L, Ali FAA, Muthumareeswaran
515 MR, et al. Removal of heavy metal ions using a carboxylated graphene oxide-
516 incorporated polyphenylsulfone nanofiltration membrane. Environ Sci Water Res
517 Technol. 2018;4(3):438–48.
518 36. Wei X, Kong X, Wang S, Xiang H, Wang J, Chen J. Removal of Heavy Metals from
519 Electroplating Wastewater by Thin- Film Composite Nano fi ltration Hollow-Fiber
520 Membranes. 2013;
521 37. Aydogan Gokturk P, Sujanani R, Qian J, Wang Y, Katz LE, Freeman BD, et al. The
522 Donnan potential revealed. Nat Commun. 2022;13(1).
523 38. Wang Y, Xu Y, Zhai W, Zhang Z, Liu Y, Cheng S, et al. In-situ growth of robust
524 superlubricated nano-skin on electrospun nanofibers for post-operative adhesion
525 prevention. Nat Commun. 2022;13(1).
526 39. Gnanasekaran G, Balaguru S, Arthanareeswaran G, Das DB. Removal of hazardous
527 material from wastewater by using metal organic framework (MOF) embedded
528 polymeric membranes. Sep Sci Technol. 2019;54(3):434–46.
529 40. Torkashvand J, Saeedi-Jurkuyeh A, Rezaei Kalantary R, Gholami M, Esrafili A,
530 Yousefi M, et al. Preparation of a cellulose acetate membrane using cigarette butt
531 recycling and investigation of its efficiency in removing heavy metals from aqueous
532 solution. Sci Rep. 2022;12(1):1–11.
533 41. Acarer-Arat S, Pir İ, Tüfekci M, Güneş-Durak S, Akman A, Tüfekci N. Heavy Metal
534 Rejection Performance and Mechanical Performance of Cellulose-Nanofibril-
535 Reinforced Cellulose Acetate Membranes. ACS Omega. 2024;
536
537
538
539

View Article Online
DOI: 10.1039/D4SU00688G

List of tables

Table 1. Composition of casting solutions

Membrane code	CA, AA and IL composition (17.5 wt. %)			Solvent (wt %)
	CA	AA	IL	DMF
M1	100%	-	-	82.5%
M2	99%	1%	-	82.5%
M3	94%	1%	5%	82.5%
M4	99%	0.5%	0.5%	82.5%

Table 2. Characteristics of wastewater

Parameters	Values
pH	6.6
TDS (ppm)	176
COD (ppm)	1580
Turbidity (NTU)	20.8
Iron (ppm)	6.65
Copper (ppm)	3.40
Lead (ppm)	4.37
Zinc (ppm)	5.19

549

550

View Article Online
DOI: 10.1039/D4SU00688G

View Article Online
DOI: 10.1039/D4SU00688G

Table 3. Contact angles of fabricated membranes

Membrane	Name of the Membranes	Water Contact Angle (°)
M1	Neat CA	51.18 ±2.1
M2	CA+ AA (1%)	68.39± 1.4
M3	CA+AA (1%) +IL (5%)	51.94± 2.4
M4	CA+AA (0.5%) +IL (0.5%)	63.0± 2.3

Table 4. Pore size of fabricated membranes

Membrane	Pore size (nm)
M1	0.0291
M2	0.0136
M3	0.0316
M4	0.0110

View Article Online
DOI: 10.1039/D4SU00688G

Table 5. Flux of Pure water and metal ion solution at pH 7 and 4 bar pressure

Membrane	Pure water flux (l/m^2 h)	Heavy metal solution flux of Copper (l/m^2 h)	Heavy metal solution flux of Magnesium (l/m^2 h)
M1	75.13	62	77
M2	32.87	15	12
M3	98.60	73	70
M4	41.09	10	12

Table 6. Rejection % of metals present in industrial wastewater

Membrane	Iron (%)	Zinc (%)	Lead (%)	Copper (%)
M1	83	71	64	73
M2	81	91	84	80
M3	83	67	76	79
M4	89	91	84	90

View Article Online
DOI: 10.1039/D4SU00688G

List of Figures

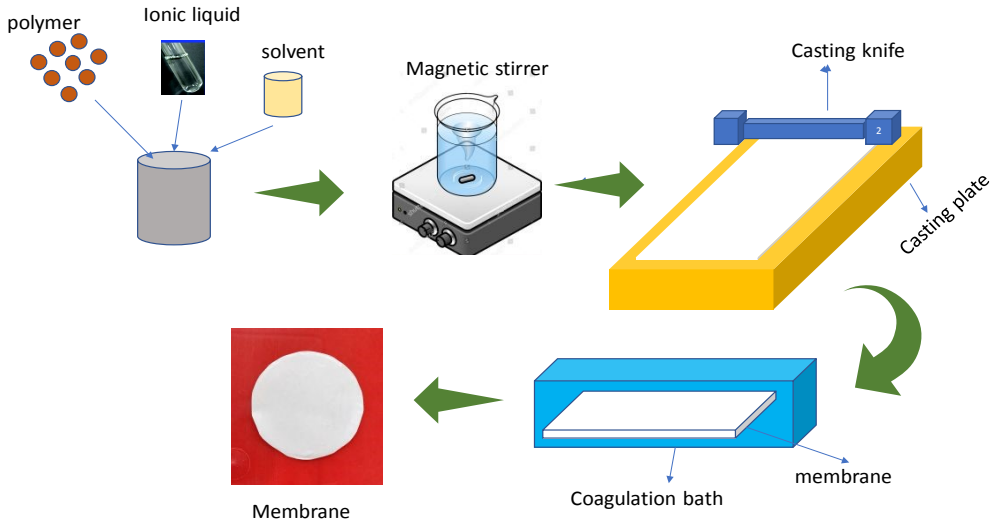

Figure 1. Fabrication of membrane

Figure 2. Nanofiltration experimental set-up

View Article Online
DOI: 10.1039/D4SU00688G

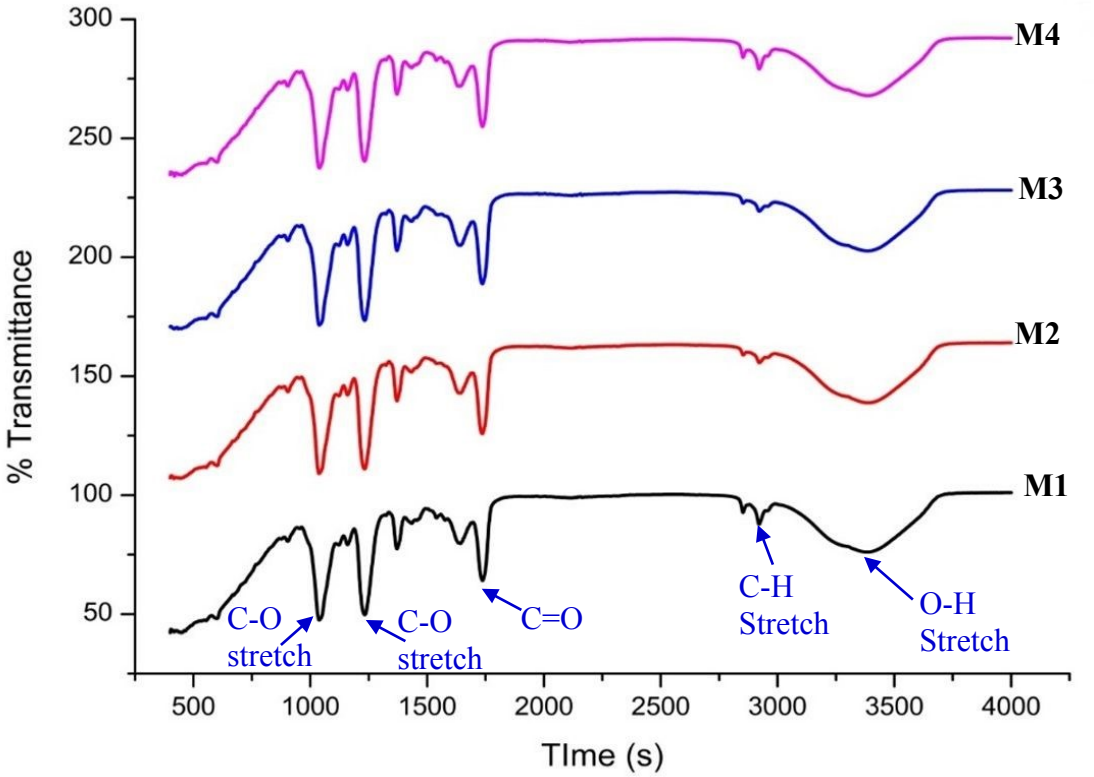

Figure 3. FTIR spectra of fabricated membranes

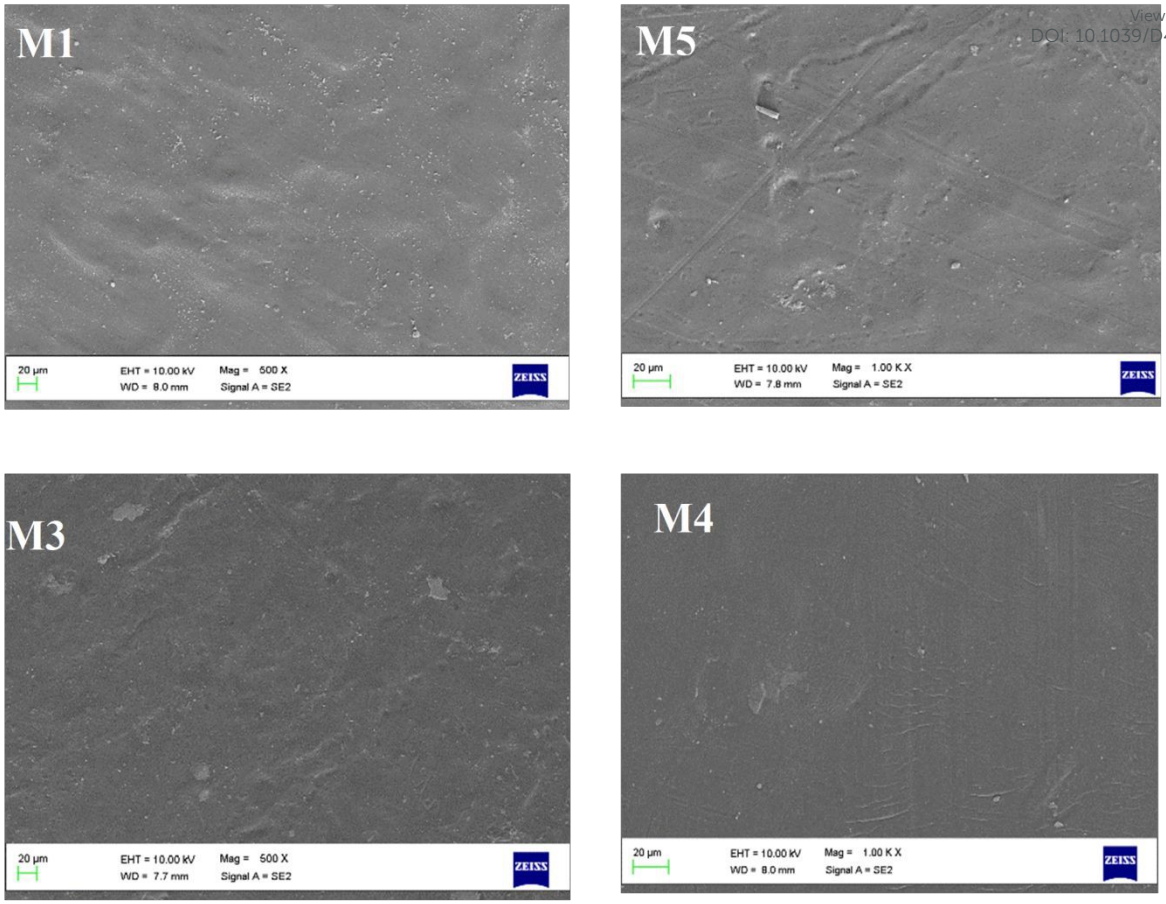

Figure 4. Surface morphology of fabricated membranes

View Article Online
DOI: 10.1039/D4SU00688G

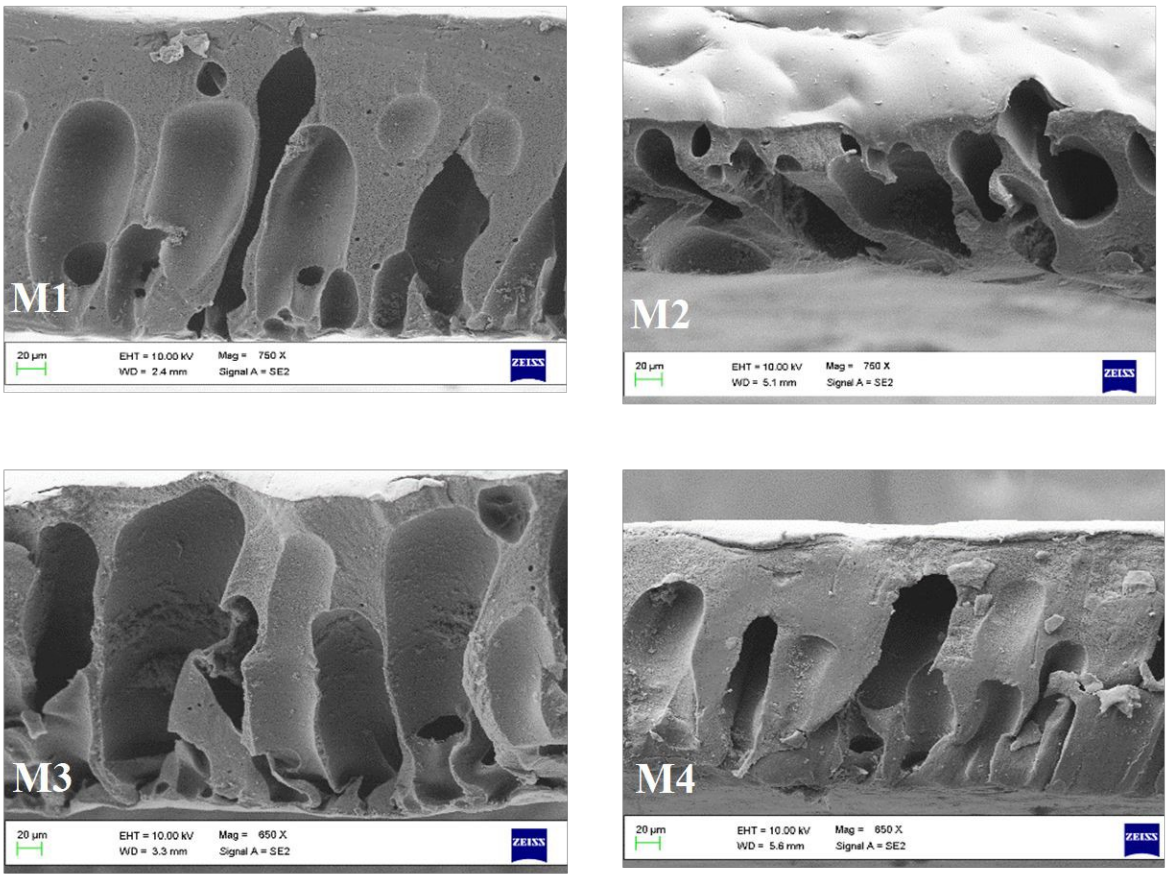

Figure 5. Cross-sectional morphology of fabricated membranes

View Article Online
DOI: 10.1039/D4SU00688G

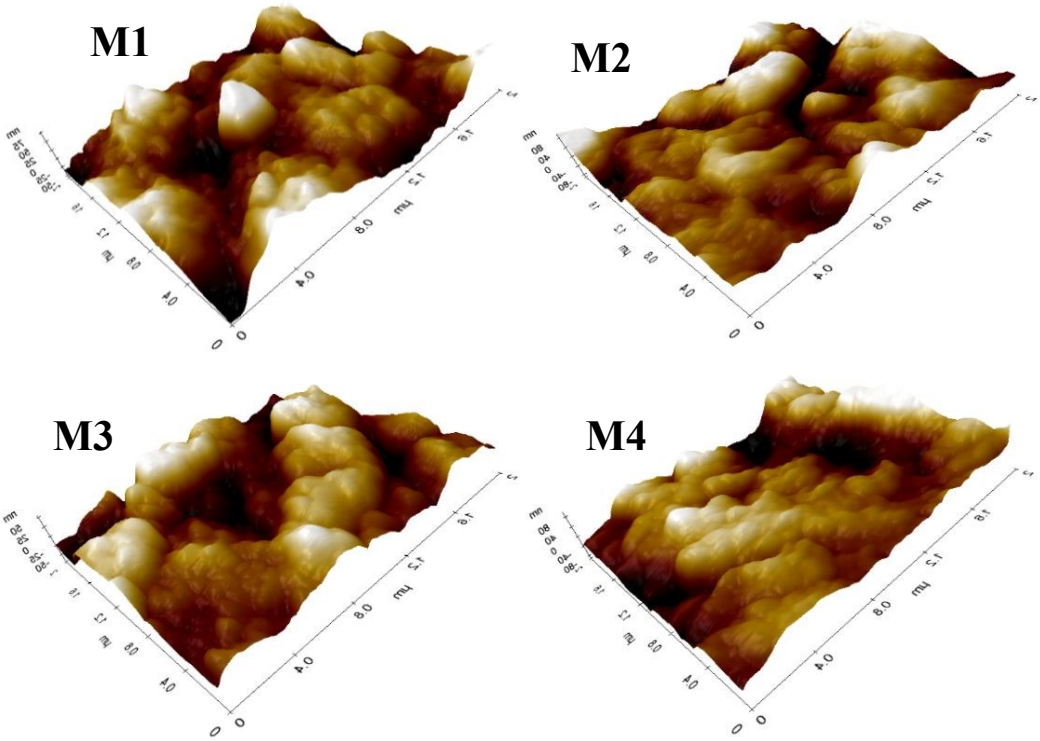

Figure 6. Surface topology of fabricated membranes

View Article Online
DOI: 10.1039/D4SU00688G

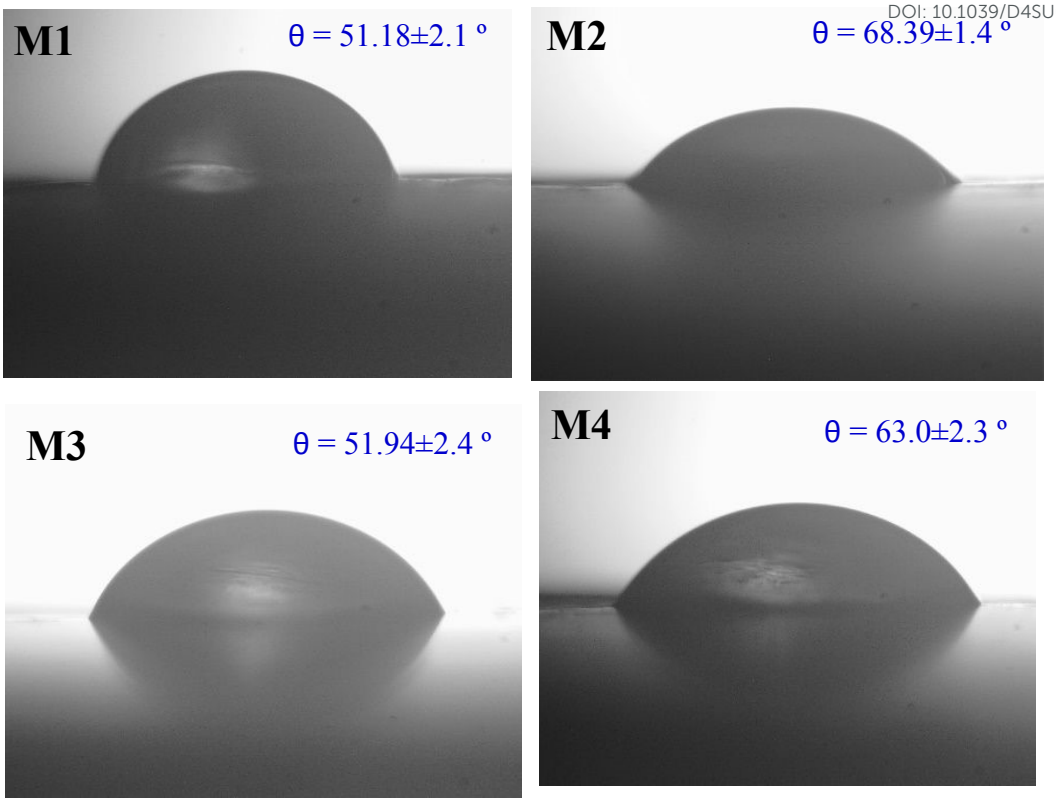

Figure 7. Contact angle images of fabricated membranes

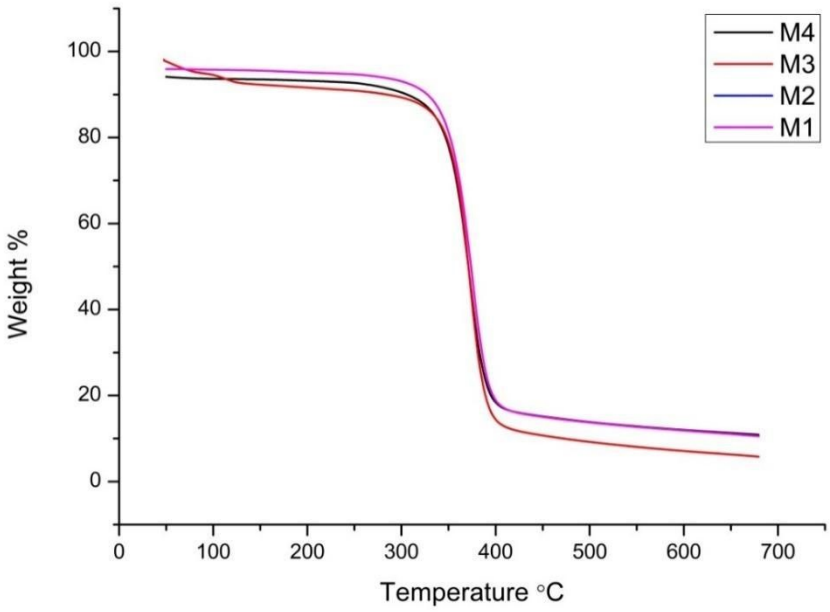

View Article Online
DOI: 10.1039/D4SU00688G

Figure 8. TGA Analysis of membranes

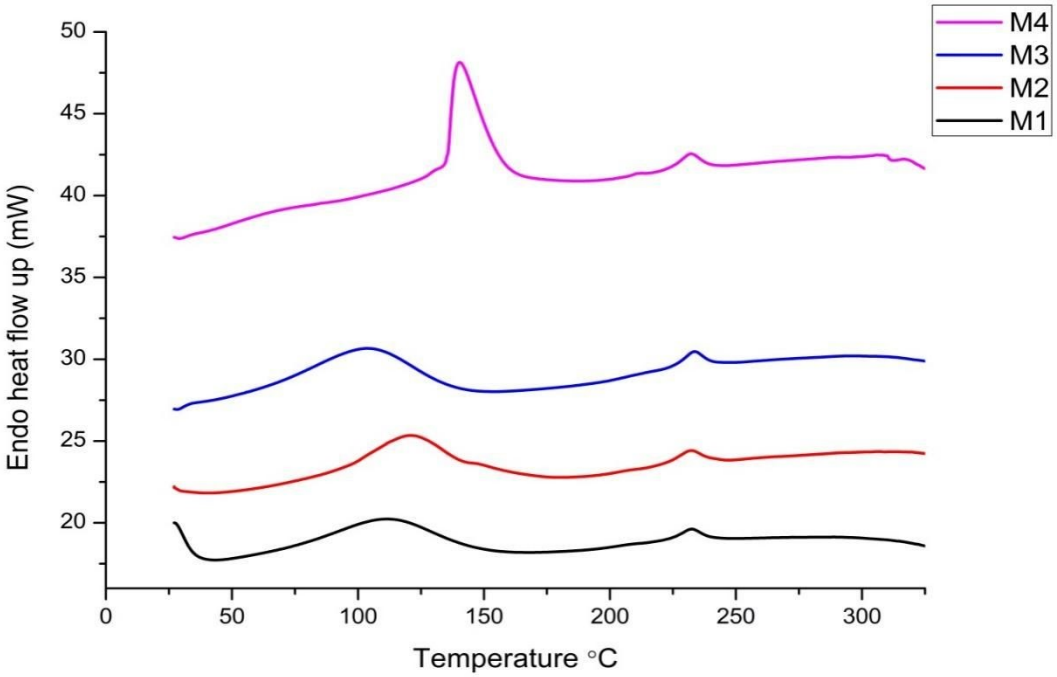

Figure 9. DSC analysis of membranes

View Article Online
DOI: 10.1039/D4SU00688G

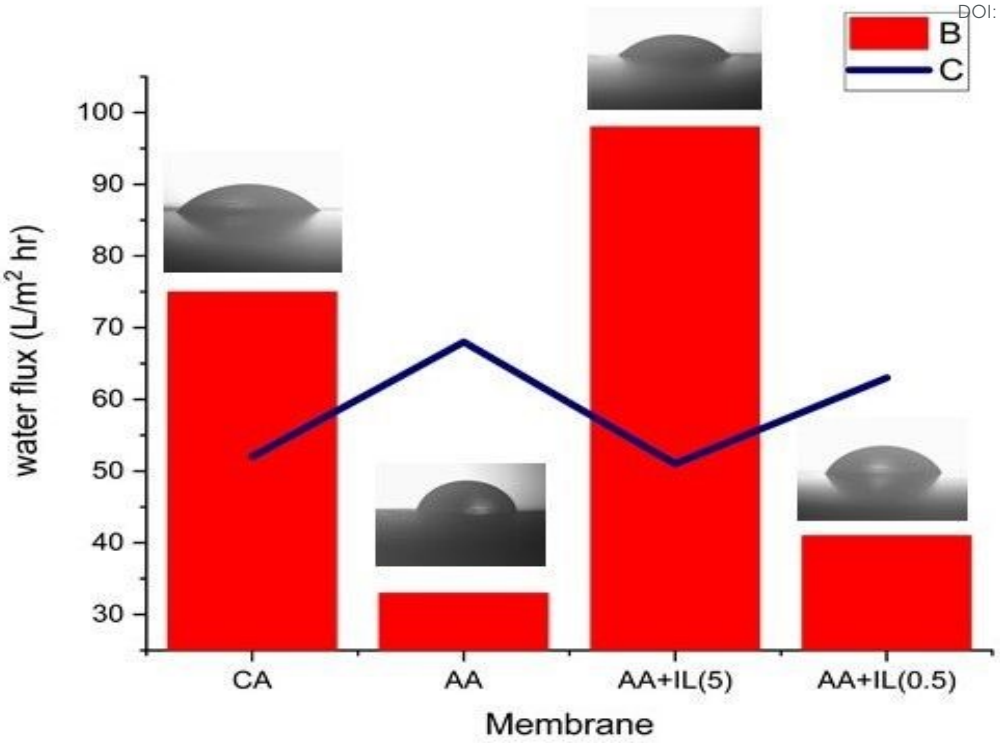

Figure 10. Pure water flux of membranes

View Article Online
DOI: 10.1039/D4SU00688G

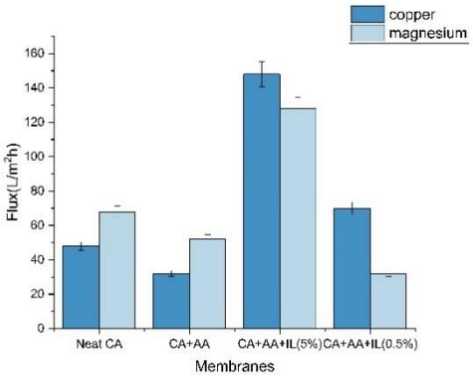

(a) NF performance of membranes at a pressure of 2 bar at pH 4

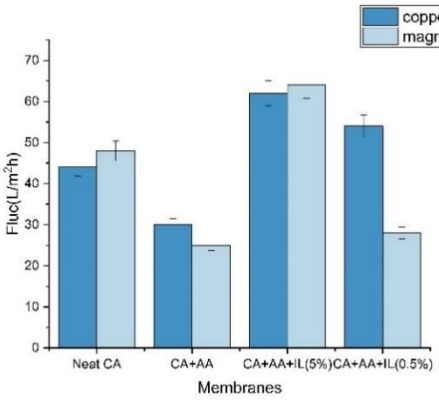

(b) NF performance of membranes at a pressure of 2 bar at pH 7

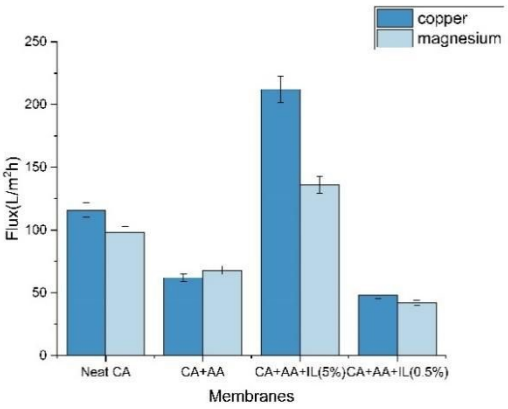

(c) NF performance of membranes at a pressure of 4 bar at pH.4

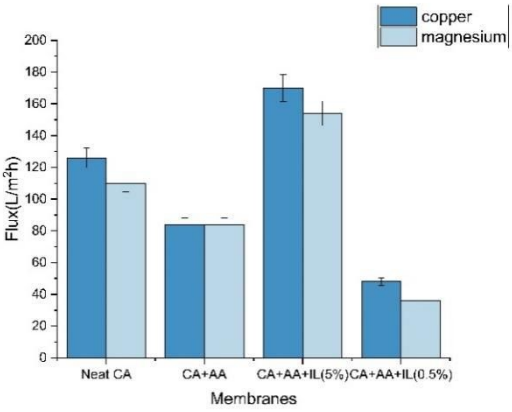

(d) NF performance of membranes at a pressure of 4 bar at pH.7

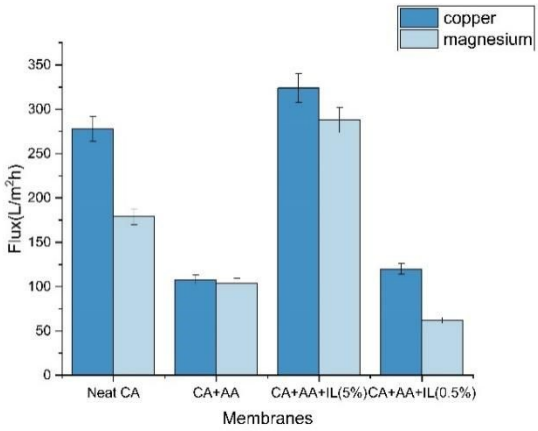

(e) NF performance of membranes at a pressure of 6 bar at pH 4

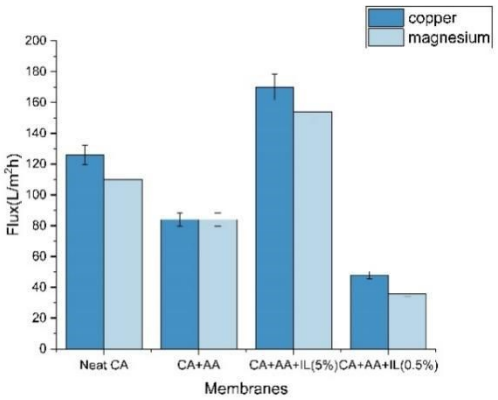

(f) NF performance of membranes at a pressure of 6 bar at pH 7

Figure 11. Flux of metal ion solution for copper and magnesium

View Article Online
DOI: 10.1039/D4SU00688G

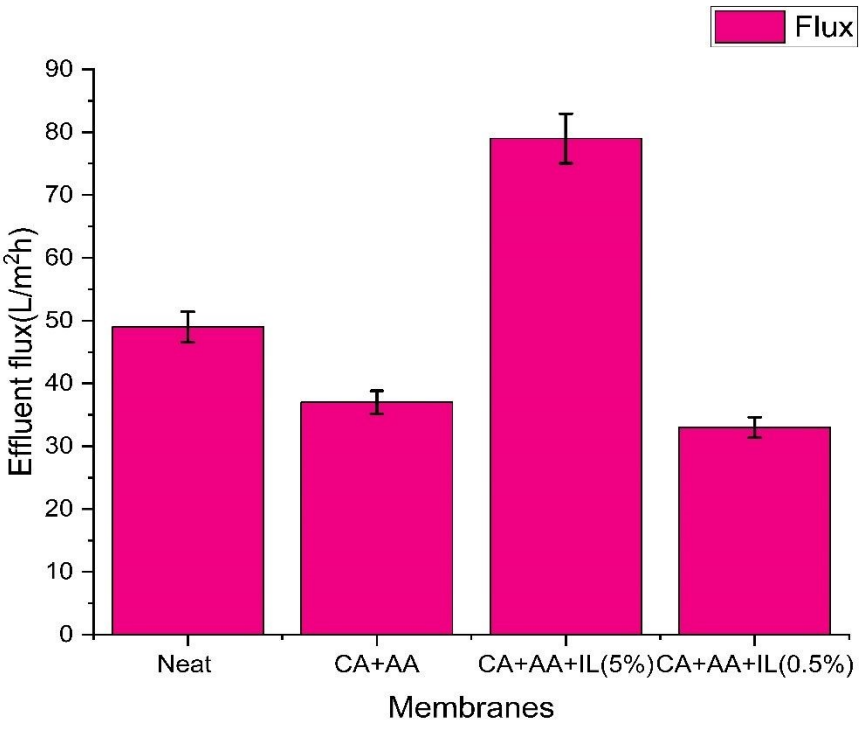

Figure 12. Nanofiltration performance of industrial wastewater

View Article Online
DOI: 10.1039/D4SU00688G

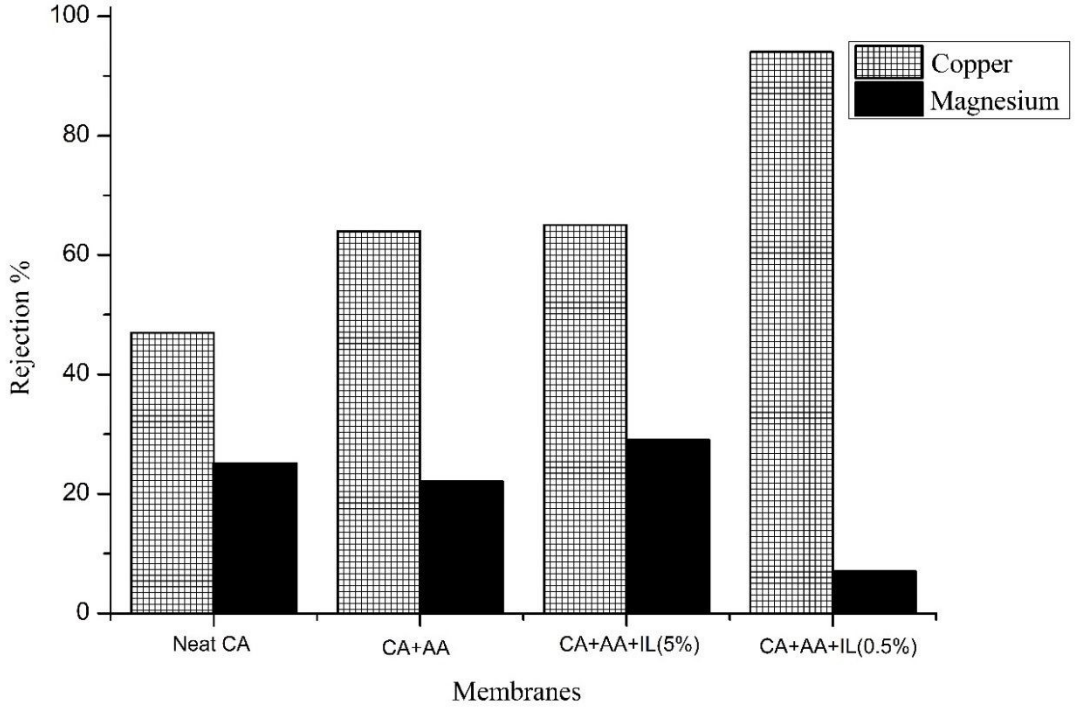

Figure 13. Rejection percentage of metal ion solution for copper and magnesium

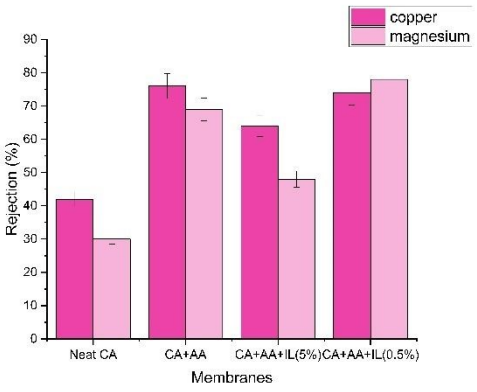

(a)Rejection performance of membranes at a pressure of 2 bar at pH 4

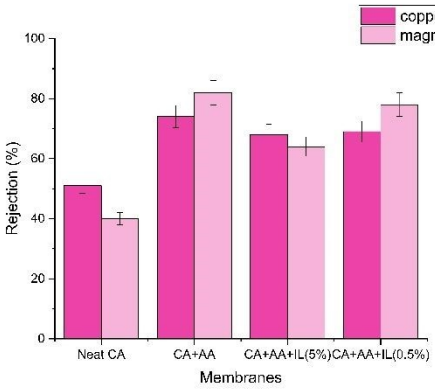

(b)Rejection performance of membranes at a pressure of 2 bar at pH 7

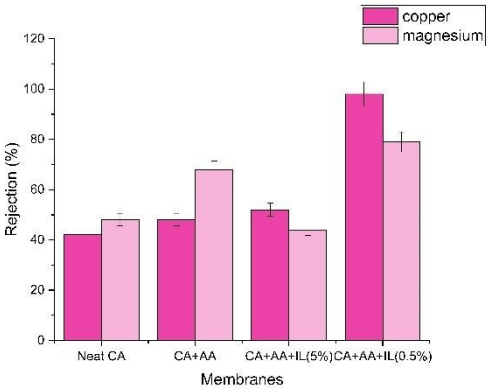

(c) Rejection performance of membranes at a pressure of 4 bar at pH 4

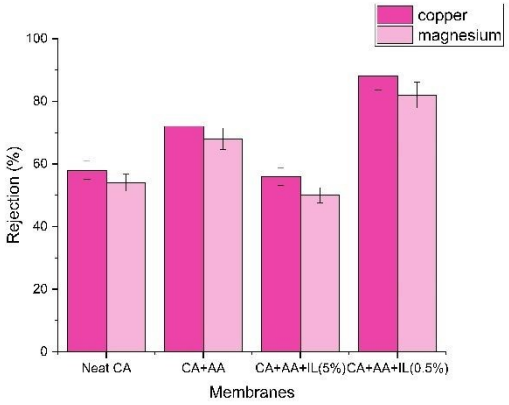

(d) Rejection performance of membranes at a pressure of 4 bar at pH 7

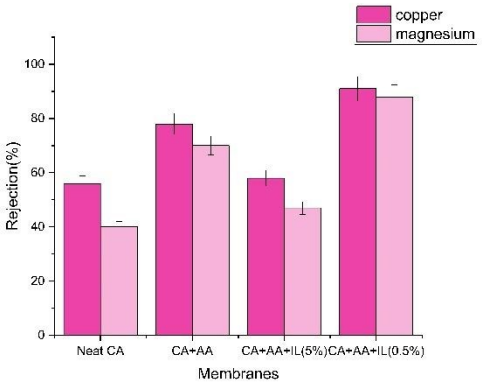

(e) Rejection performance of membranes at a pressure of 6 bar at pH 4

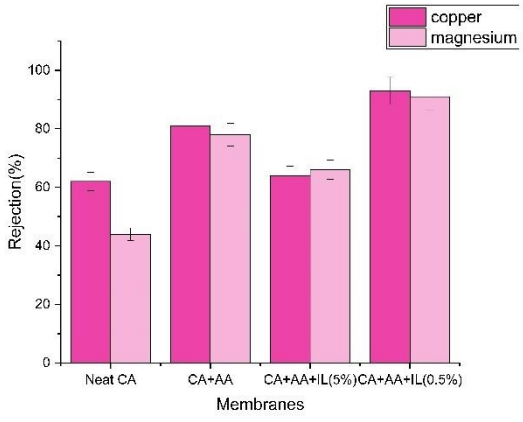

(a) Rejection performance of membranes at a pressure of 6 bar at pH 7

Figure 14. Rejection percentage of metal ion solution for Copper and Magnesium at different pressures and pH

View Article Online
DOI: 10.1039/D4SU00688G

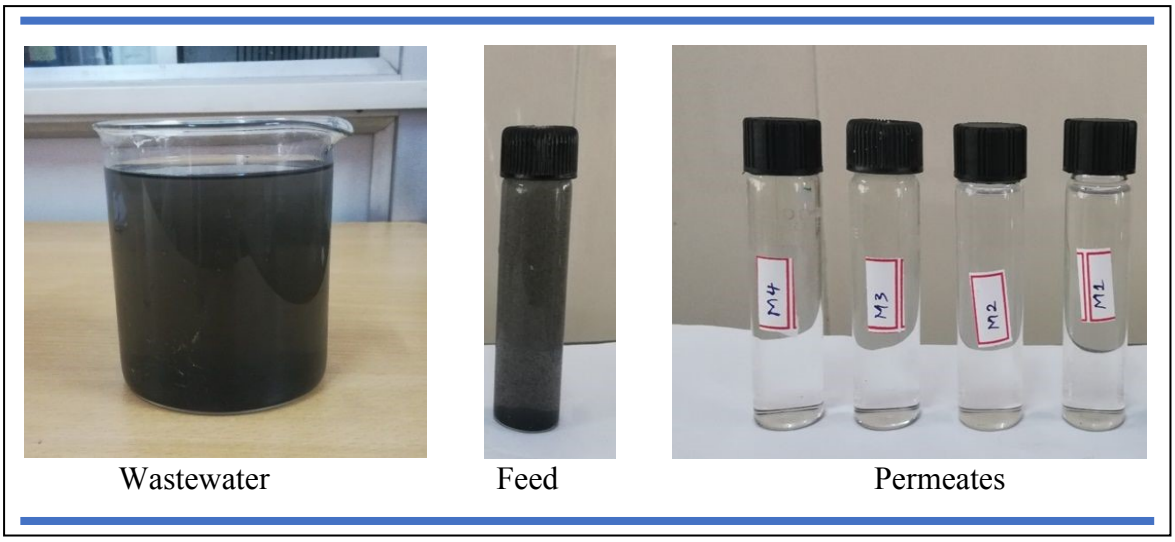

Figure 15: Feed and permeate of wastewater

View Article Online
DOI: 10.1039/D4SU00688G

Data availability statements

The authors confirm that the data supporting the findings of this study are available within the article. Should any raw data files be needed in another format they are available from the corresponding author upon reasonable request.